

# The Extreme Ultraviolet Spectrum of the Kinetically Dominated Quasar 3C 270.1

Brian Punsly and Paola Marziani

*1415 Granvia Altamira, Palos Verdes Estates CA, USA 90274 and ICRANet, Piazza della Repubblica 10 Pescara 65100, Italy*

*INAF, Osservatorio Astronomico di Padova, Italia.*

*E-mail: brian.punsly1@verizon.net*

14 July 2021

## ABSTRACT

Only a handful of quasars have been identified as kinetically dominated, their long term time averaged jet power,  $\bar{Q}$ , exceeds the bolometric thermal emission,  $L_{bol}$ , associated with the accretion flow. This letter presents the first extreme ultraviolet (EUV) spectrum of a kinetically dominated quasar, 3C 270.1. The EUV continuum flux density of 3C 270.1 is very steep,  $F_\nu \sim \nu^{-\alpha_{EUV}}$ ,  $\alpha_{EUV} = 2.98 \pm 0.15$ . This value is consistent with the correlation of  $\bar{Q}/L_{bol}$  and  $\alpha_{EUV}$  found in previous studies of the EUV continuum of quasars, the EUV deficit of radio loud quasars. Curiously, although ultraviolet broad absorption line (BAL) troughs in quasar spectra are anti-correlated with  $\bar{Q}$ , 3C 270.1 has been considered a BAL quasar based on an SDSS spectrum. This claim is examined in terms of the EUV spectrum of OVI 1 and the highest resolution CIV spectrum in the archival data and the SDSS spectrum. First, from [OIII]4959,5007 (IR) observations and the UV spectral lines, it is concluded that the correct redshift for 3C 270.1 is 1.5266. It is then found that the standard measure of broad absorption,  $BAL_{nicity} = 0$ , for MgII 2800, CIV 1549 and OVI 1032 in all epochs.

**Key words:** Black hole physics — magnetohydrodynamics (MHD) — galaxies: jets—galaxies: active — accretion, accretion disks

The quasar 3C 270.1 contains one of the most powerful jets of any known active galactic nucleus. The jet power greatly exceeds any other associated with a quasar that has been claimed to have an ultraviolet (UV) broad absorption line. These extreme properties of 3C 270.1 offer a unique laboratory for exploring the mechanism of relativistic jet formation. The long term time averaged jet power,  $\bar{Q}$ , determined from low frequency radio lobe emission, is so extreme that the quasar was classified as kinetically dominated  $\bar{Q}/L_{bol} > 1$ , where  $L_{bol}$  is the bolometric thermal emission associated with the accretion flow (Punsly 2007). The physical relevance of this result is uncertain since the plasma in the radio lobes was ejected from the central engine  $> 10^5$  years before the UV emitting gas reached the environs of the central black hole. This letter uses the EUV spectrum of 3C 270.1 to address two fundamental issues. First, can a quasar actually emit more power in the jet than is being radiated as thermal emission? Secondly, why are broad absorption line winds anti-correlated with jet emission on super-galactic scales? Both of the issues provide valuable clues to the jet launching mechanism.

Even though the radio lobes of powerful radio loud

quasars (RLQs) are located light travel times typically  $10^5$  -  $10^6$  yrs from the central black hole, they tend to be connected by a radio jet. Quasars with radio lobes on supergalactic scales are very rare,  $\sim 1.7\%$  of all quasars have such extended structure (deVries et al. 2006). The existence of the connective bridge formed by the jet implies that the energy source seems persistent for long periods of time. It is a mystery how the jet can be powered for so long and it is unclear how much the jet power fluctuates over  $10^6$  yrs compared to its average value. In Punsly (2014, 2015), it was shown that  $\bar{Q}/L_{bol}$  (which depends on a long term average) was correlated with the deficit of EUV emission quantified by  $\alpha_{EUV}$  (the flux density scales as  $F_\nu \propto \nu^{-\alpha_{EUV}}$ ). The EUV is believed to be the putative Wien tail of the optically thick emission from the innermost region of the accretion flow; a region of the flow that interacts in real time with the central black hole (Punsly 2015). Like the bridge formed by the jet, this also seems to indicate a rather persistent dynamic near the central black hole that is sustained for most of  $\sim 10^6$  yrs of the radio source lifetime. Furthermore, there is only a modest degree of scatter from the average trend in the  $\bar{Q}/L_{bol} - \alpha_{EUV}$  plane (see Figure 2) for the RLQ popu-

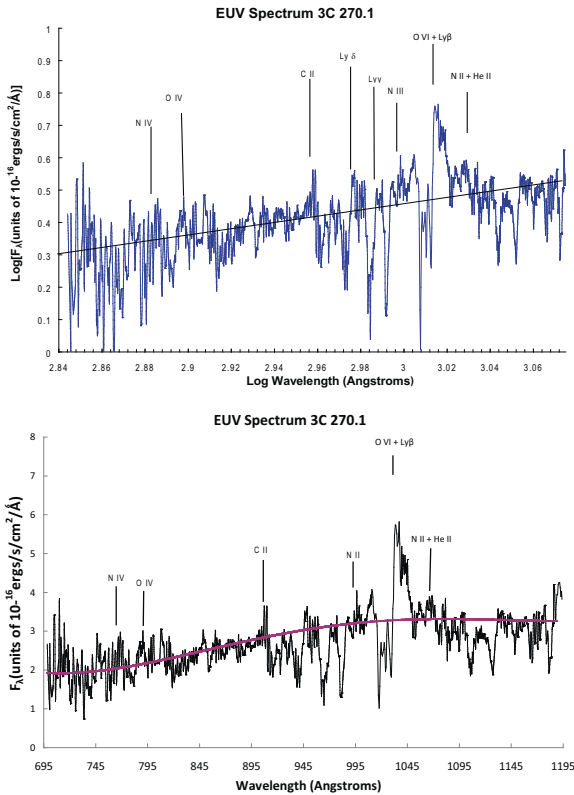


**Figure 1.** The EUV spectrum of 3C 270.1. The top frame is the power law fit (solid black line) to the continuum. The bottom frame is a fourth order polynomial fit (solid red line) to the continuum.

lation. The scatter plot samples quasars at random epochs in their radio loud lifetime. This modest scatter indicates that the fluctuations in the dynamics are typically not that large. Some “baseline” dynamical configuration seems to exist in each quasar more often than not for the majority of these objects. In the next section, this is interpreted with other evidence to indicate that 3C 270.1 had a powerful jet,  $Q(t)/L_{bol} \sim 1$ , when the EUV radiation was emitted.

Another aspect of this study is to analyze the claim of Gibson et al. (2009) that 3C 270.1 has broad absorption in CIV and not associated absorption. This conclusion contradicts previous findings (Anderson et al 1987). This is physically significant since there are only a handful of known RLQs with extended structure on super-galactic scales that are bona-fide BALQSOs as defined by the BALnicity index. None of these have  $\overline{Q}/L_{bol}$  within a factor of 10 of 3C 270.1. This conflict is analyzed in Section 2. Quantifying the jet power and the interplay between the BAL wind suppression and jet power provides fundamental insight into the nature of the jet launching in quasars.

## 1 THE EUV SPECTRUM AND JET POWER

3C 270.1 was observed on 7/24/2000 for 2380 s with the Hubble Space Telescope (HST) with the STIS spectrograph and G230L grating. The data was downloaded from MAST and corrected for Galactic extinction with the CCM ab-

sorption law (Cardelli et al. 1989). The absorption from the Ly $\alpha$  valley was de-convolved from the data using the empirical statistical methods of (Zheng et al. 1997). An intervening Lyman limit system near the quasar systemic redshift was removed with the decrement method (Shull et al. 2012; Punsly 2014). Namely, the Lyman limit system was removed by assuming a single cloud with a  $\nu^{-3}$  opacity and an absorption that was scaled by the decrement between the continuum and the trough depth. This was considered acceptable because the power law above the Lyman limit system continues smoothly through the corrected region (see Figure 1). The power law between 1100Å and 700Å is defined by  $\alpha_{EUV} = 2.98 \pm 0.15$ . The top frame of Figure 1 is the power law fit (solid black line) to the continuum. The bottom frame is a fourth order polynomial fit (solid red line) that provides an upper limit to the continuum in the analysis of OVI absorption in the next section.

A method that allows one to convert 151 MHz flux densities,  $F_{151}$  (measured in Jy), into estimates of long term time averaged jet power,  $\overline{Q}$ , (measured in ergs/s) is given by Equation (1) (Willott et al. 1999; Punsly 2005):

$$\begin{aligned} \overline{Q} &\approx [(\mathbf{f}/15)^{3/2}] 1.1 \times 10^{45} [X^{1+\alpha} Z^2 F_{151}]^{0.857} \text{ ergs/s} \quad (1) \\ Z &\equiv 3.31 - (3.65) \times \\ &[X^4 - 0.203X^3 + 0.749X^2 + 0.444X + 0.205]^{-0.125} \quad (2) \end{aligned}$$

where  $X \equiv 1 + z$ ,  $F_{151}$  is the total optically thin flux density from the lobes. Deviations from the overly simplified minimum energy estimates are combined into a multiplicative factor,  $\mathbf{f}$ , that represents the small departures from minimum energy, geometric effects, filling factors, protonic contributions and low frequency cutoff (Willott et al. 1999). In Blundell and Rawlings (2000), it was argued that  $10 < \mathbf{f} < 20$ . Alternatively, there is another isotropic estimator in which the lobe energy is primarily inertial in form (Punsly 2005):

$$\overline{Q} \approx 5.7 \times 10^{44} (1 + z)^{1+\alpha} Z^2 F_{151} \text{ ergs/sec} . \quad (3)$$

Define the radio spectral index,  $\alpha$ , as  $F_\nu \propto \nu^{-\alpha}$ . Equation (1) with  $\mathbf{f} = 20$  is the maximum upper bound on  $\overline{Q}$  and Equation (2) is the lower bound  $\overline{Q}$  that is used in the following. In this paper, we adopt the following cosmological parameters:  $H_0=70$  km/s/Mpc,  $\Omega_\Lambda = 0.7$  and  $\Omega_m = 0.3$ . The radio images in Garrington et al. (1991) indicate that this is a lobe dominated quasar. Therefore, one expects the 151 MHz flux density (14.96 Jy from the NASA Extragalactic Database) to be dominated by the radio lobe emission. Thus, from Equations (1) - (3) that  $\overline{Q} = 7.5 \times 10^{46} \pm 1.5 \times 10^{46}$  erg/s.

Since the data used here covers the peak of the SED at  $\lambda \approx 1100\text{\AA}$ , an accurate expression,  $L_{bol} \approx 3.8\lambda L_\lambda$  ( $\lambda = 1100\text{\AA}$ ), can be used to estimate the accretion disk luminosity. This does not include reprocessed IR emission in distant molecular clouds (Davis and Laor 2011; Punsly 2014). From the flux density in Figure 1,  $L_{bol} = 5.2 \times 10^{46} \pm 0.5 \times 10^{46}$  erg/s. Combining this with the estimate of  $\overline{Q}$ , above,  $\overline{Q}/L_{bol} = 1.4$ . 3C 270.1 is kinetically dominated in this context.

The top frame of Figure 2 places 3C 270.1 on the same scatter plot of  $\log[\overline{Q}/L_{bol}]$  and  $\alpha_{EUV}$  as the other quasars for which a similar data reduction was performed in Figure 3 of Punsly (2015). 3C 270.1 has the most powerful jet and

it lies at the end of the extrapolated trend of the other powerful RLQs. Figure 2 relates real time properties (meaning concurrent with the epoch that the data was sampled in the quasar rest frame),  $L_{bol}$  and  $\alpha_{EUV}$ , with a long term time average property,  $\overline{Q}$ . The coefficient of determination to a linear fit is 0.5927 so the scatter is modest. Each data point in Figure 2 is a random snapshot in time of the properties of the innermost accretion flow during the lifetime each RLQ. The degree of scatter indicates that there is a baseline or fiducial configuration of the central engine in each RLQ and the fluctuations over time from this configuration are usually “modest” and large fluctuations are not typical. This concept is quantified below in order to see if there is predictive power of real time jet parameters from the data in Figure 2. To begin with, segregate the real time variables from  $\overline{Q}$  by inverting the linear fit to the data in the top frame of Figure 2. This process yields a real time variable

$$G(t) = 2.58\alpha_{EUV}(t) + \log[3.8\lambda L_{\lambda}(\lambda = 1100\text{\AA})(t)/10^{45}\text{ergs/s}]. \quad (4)$$

As an alternative to a scatter plot in the  $\log[\overline{Q}/L_{bol}] - \alpha_{EUV}$  plane (the top frame of Figure 2), one can also consider the data scatter in the  $\log[\overline{Q}] - G(t)$  plane. Define  $\overline{\Psi}$  as the best fit power law estimator of  $\log(\overline{Q})$  in the new scatter plane. Then

$$\overline{\Psi} = 38.97G(t)^{0.0815}, \quad (5)$$

and the coefficient of determination is 0.5937.

In order to extract the predictive capability of Equation (5) for the real time jet power (that which is concurrent with the EUV measurements),  $Q(t)$ , consider the following. The EUV emission and the jet launching both originate in the immediate vicinity of the central supermassive black hole Punsly (2015). The fundamental assumption of this analysis is: *Since the EUV and the jet emanate from a common compact region, the correlation found in Figure 2 between these powerful dynamic elements is not spurious or coincidental, but results from an actual physical connection between,  $\alpha_{EUV}(t)$ ,  $L_{bol}(t)$  and  $Q(t)$  in real time.* In particular, the average trend in Figure 2 is a direct consequence of this real time interaction, or alternatively stated Equation (5) is a consequence of a more fundamental quasi-simultaneous relation

$$\log Q(t) = 38.97G(t)^{0.0815}. \quad (6)$$

However, this relationship can only true in an average sense due to variations from RLQ to RLQ, and epoch to epoch variations in both the geometry as well as the physical state of the innermost accretion flow. Describe the stochastic behavior of  $\log(Q(t))$  by a probability distribution,  $\Psi\{Q[G(t)]\}$ , that represents the physics of a complicated dynamical system created by an ensemble of numerous microphysical domains. From Equations (5) and (6), the mean of the distribution is,  $\mu[\Psi\{Q[G(t)]\}] \equiv \overline{\Psi} = 38.97G^{0.0815}$ , where  $G$  is the time average of  $G(t)$ . To estimate the variance of  $\Psi\{Q[G(t)]\}$ , note that each data point in Figure 2 is a random time snapshot of the inner most accretion flow, so the best fit to the trend represents the time averaged configuration for a given  $\log(\overline{Q})$  and the dispersion from this trend results from  $G(t)$  (and therefore  $Q(t)$  by Equation (6)) varying from the mean value. From the scatter in the  $\log[\overline{Q}] - \log Q(t)$  plane, one can compute the standard deviation,  $\sigma = 0.46$ . Assuming a normal distribution,  $Z$ ,

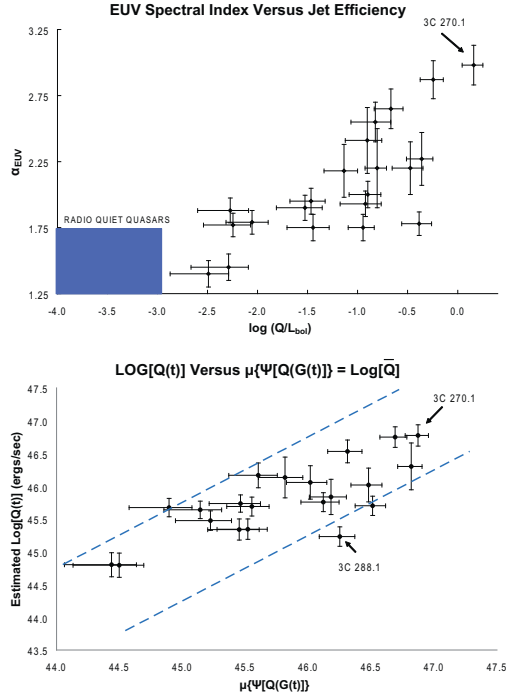


**Figure 2.** The top frame is a scatter plot of  $\overline{Q}/L_{bol}$  vs.  $\alpha_{EUV}$ . The bottom frame is a scatter plot of  $Q(t)$  estimated from Equation (6) relative to the 90% confidence contours (blue dashed) of the probability distribution,  $\Psi\{Q[G(t)]\}$ , in Equation (7).

$$\Psi\{Q[G(t)]\} = Z[\mu = 38.97G^{0.0815}, \sigma = 0.46]. \quad (7)$$

Based on the confidence contours (computed from  $\Psi\{Q[G(t)]\}$ ), plotted as dashed blue curves in the bottom frame of Figure 2,  $7.3 \times 10^{45}\text{ergs/s} < Q(t) < 4.8 \times 10^{47}\text{ergs/s}$  with 90% confidence. A large  $Q(t)$  is consistent with the existence of a powerful radio core  $\approx 4.9 \times 10^{44}\text{ergs/s}$  (Lonsdale et al. 1993; Akujor et al. 1994; Garrington et al. 1991).

As a verification of the validity of this method consider, the outlier in Figure 2, 3C 288.1. The EUV deficit is much less than expected for the value of  $\overline{Q}$ . However, the radio core is rather weak with a 1 GHz - 100 GHz luminosity of  $\approx 1.0 \times 10^{43}\text{ergs/s}$  (Reid et al. 1995). The source has very little intrinsic absorption as evidenced by the flat EUV spectral index, so one expects a direct line of sight to the core. This implies that it is an intrinsically weak radio core with no significant free-free absorption or Doppler de-boosting. The conclusion is that 3C 288.1 is an outlier in Figure 2 because the quasar is currently in a state of relatively weak radio activity.

## 2 UV EMISSION LINES AND ABSORPTION LINES

One of the most striking trends in the quasar phenomenon is that the broad absorption line prominence is anti-correlated with the radio loudness of the quasar (Becker et al. 2001; Shankar et al. 2008). If one considers RLQs with extended emission on super-galactic scales (radio lobes) this anti-correlation is stronger. Only a handful of BALQSO can-

didates with extended radio emission have ever been found even in deep surveys (Gregg et al. 2006). Considering the large jet power in 3C 270.1, the claim of Gibson et al. (2009) that there was a CIV BAL in the SDSS spectrum (under the formal definition of Weymann et al. (1991) per Equation (8), below) is startling. Even more so because the absorption of CIV in 3C 270.1 was analyzed by R. Weymann in Anderson et al (1987) and was an example of what is not a BAL, but what they call associated absorption. Since the anti-correlation between the power of extended radio lobes and BALs is likely related to the phenomenon of jet launching and BAL wind formation, this controversial finding is examined in detail in this section. The top frame of Figure 3 is an overlay of the MMT (Multiple Mirror telescope) data from Anderson et al (1987) and the SDSS data (see also Table 1). The OVI absorption is displayed in the bottom frame of Figure 3. The upper limit of the continuum is solid red (the fourth order polynomial fit) and the blue dashed line is the power law fit from Figure 1. It is clearly broader and higher velocity than the CIV absorber. The data was plotted with a smoothing window of  $1.25\text{\AA}$  in the quasar rest frame.

The BALnicity index, BI, was defined in Weymann et al. (1991) as

$$BI = \int_{v=-25000}^{v=-3000} [1 - F(v)/0.9] C dv, \quad (8)$$

where  $F(v)$  is the flux density normalized to the continuum level as a function of  $v$ , the velocity from the QSO rest frame line emission frequency in km/s. The step function,  $C(v) \neq 0$  if and only if there more than 2000 km/s of continuous absorption beyond -3000 km/s. This measure of broad absorption has been borne out over the years as very robust. More lax measures of absorption (such as associated absorption and mini-BALs) have turned out to represent different classes of objects, that have less X-ray absorption than BALQSOs and larger radio luminosity than bona-fide BALQSOs (Shankar et al. 2008; Punsly 2006; Knigge et al. 2008). In deriving this measure, the authors considered narrower associated absorption and decided that this was a different phenomenon. The function  $C(v)$  was designed to segregate out this type of absorption.

In order to implement Equation (8), we need an accurate determination of the redshift. From the [OIII] narrow lines observed in Jackson and Rawlings (1997), we obtain  $z = 1.5226$ . This agrees with our UV line analysis of the SDSS data,  $1.5228 \pm 0.0013$  at the  $1\sigma$  confidence level.  $C \neq 0$  requires absorption beyond -5000 km/s. Thus, from Figure 3 and Table 1, there is no absorption beyond -5000 km/s and  $C = 0$  for CIV and OVI for all  $v$ . These absorption have  $BI = 0$  and are examples of associated absorption that is common in RLQs.

OVI shows absorption maxima at  $v \approx -4290, -2480$  km/s and CIV shows absorption at  $v \approx -2660$  km/s. From the data in Aldcroft et al. (1994) and the SDSS data in Table 1, the narrow MgII absorption arises from gas that has an outflow velocity of  $v \approx -2620$  km/sec. This indicates the following wind dynamic. There is a narrow absorption line wind with  $v_{\text{wind}} \approx 2600$  km/s and second high ionization wind with  $v_{\text{wind}} \approx 4300$  km/s. It is not clear if the high ionization wind is the base of a common wind that coasts at  $v_{\text{wind}} \approx 2600$  km/s farther out.

The UV emission lines were decomposed into a broad,

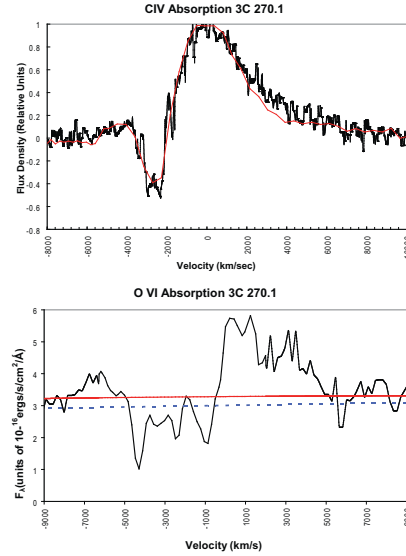


**Figure 3.** Ultraviolet absorption lines occur in the spectrum. The CIV line as measured by MMT is plotted in black in the top frame. The SDSS low resolution CIV spectrum is overlaid in red. The data is referenced to the estimated continuum level. The OVI absorption and emission line is plotted in the bottom frame. The solid red line is the fourth order polynomial fit and the dashed blue line is the power law fit to the continuum.

a very broad and narrow components as has been previously documented in the analysis of eigenvector 1 and the Population A/B dichotomy used to classify quasar spectrum (Sulentic et al. 2007). It is demonstrated that the line profiles are typical of RLQ, Pop. B sources which are at the opposite end of eigenvector 1 from the BALQSOs (Pop. A sources). From Table 1, the peaks of the CIV, CIII] and MgII broad components show small redshifts relative to the quasar systemic velocity consistent with Pop B sources (Sulentic et al. 2007). Secondly, here is a tendency for redward asymmetric profiles which is also associated with RLQ, Pop. B sources. Using the measure for asymmetry from Wills et al. (1995),  $A$ , that is defined in terms of the full width half maximum, FWHM, in  $\text{\AA}$ ; the midpoint of an imaginary line connecting a point defined at 1/4 of the peak flux density of the BEL on the red side of the BEL to 1/4 of the peak flux density on the blue side of the BEL,  $\lambda_{25}$ , and a similar midpoint defined at 8/10 of the flux density maximum,  $\lambda_{80}$ , as

$$A = \frac{\lambda_{25} - \lambda_{80}}{FWHM}. \quad (9)$$

A positive value of  $A$  means that there is excess flux in the red broad wing of the emission line. The redward asymmetry, especially of CIV, has been previously associated with radio loud quasars (Punsly 2010). The values in Table 1 are large even for RLQs. Finally, the small intensity ratio Al III 1860 / CIII] 1909  $\approx 0.08$  is typical of Pop. B sources (Bachev et al. 2004). The designation as a Pop. B source is consistent with the Mg II and CIV absorption widths in Table 1. The narrow widths are typical of narrow absorption lines not broad absorption lines.

Using the MgII broad component width from Table 1, we obtain mass estimates for the central black hole

**Table 1.** Prominent Emission Lines Properties from the SDSS Spectrum

Line	Broad Component FWHM (km/s)	Full Line FWHM (km/s)	Line Shift km/s	Redward Asymmetry A	Absorption FWHM (km/s)	Absorption Velocity km/s	Notes
Mg II	3060	4110	440	0.32	305/370	-2632/-2609	1
C III	3702	4290	430	0	0	...	..
C IV	3070	3870	265	0.15/0.24	1200	-2663	2

1. The two absorption widths are from resolved doublet 2. The larger asymmetry is from Anderson et al (1987) as seen in Figure 3.

$\log M_{bh} = 8.89$  and  $\log M_{bh} = 8.99$  from the methods of Shen and Liu (2012) and Trakhtenbrot & Netzer (2012), respectively. Combining these estimates with  $L_{bol}$  from Section 1 indicates an Eddington rate,  $L_{bol} = 0.48 \pm 0.10 L_{Edd}$ . This is very high for a Pop. B source and is more typical of a Pop. A, radio quiet source. Thus, 3C 270.1 is extreme in all its properties, a very strong jet and a very luminous accretion disk.

### 3 CONCLUSION

In the first section, the EUV spectrum of 3C 270.1 was found to have  $\alpha_{EUV} = 2.98 \pm 0.15$ . It was shown that 3C 270.1 has all the properties associated with the one of the most powerful RLQ jets in the known Universe. An argument was made that the  $\log[\bar{Q}] - \alpha_{EUV}$  scatter plane (Figure 2) can be used to estimate a confidence interval for real time jet power,  $Q(t)$ . Unlike other correlations in the literature involving  $\bar{Q}$ , such as with emission line properties as in Willott et al. (1999), it was noted that both the EUV and  $Q(t)$  originate from near the central black hole and the correlation in the  $\log[\bar{Q}/L_{bol}] - \alpha_{EUV}$  scatter plane therefore indicates a nearly simultaneous causal contact between the two dynamical processes. If not for this circumstance, the estimator for  $Q(t)$  would be unjustified. The method developed here might have application to other extreme quasars in future studies. In the second section, it was shown that the CIV and OVI absorption had  $BI = 0$ . Thus, 3C 270.1 is not a broad absorption line quasar as classically defined, but displays the well known associated absorption that occurs in many RLQs.

The details of the correlation found in Figure 2 was elucidated in two previous studies. Firstly, a correlation induced by larger black hole masses and lower accretion rates in RLQs was ruled out empirically as a plausible explanation due to the indistinguishable SED peak in RLQs and RQQs (Punsly 2014). A partial correlation analysis in Punsly (2015) indicates that the fundamental physical correlation amongst quantities is between  $Q/L_{bol}$  and  $\alpha_{EUV}$ . This correlation is not explained by the Laor and Davis (2014) disk wind. However, as discussed in Punsly (2014) the most likely explanation of the correlation, jets from magnetic flux in the inner accretion disk, can coexist with these winds. Consistent 3-D MHD numerical models are those in which an annular region ( $\sim 2-4$  black hole radii wide) of the innermost accretion flow, adjacent to the black hole, is perforated by islands of large scale poloidal (vertical) magnetic flux. The rotating flux distribution associated with the magnetic islands is the source of the relativistic jet and it also displaces the EUV emitting gas, thereby causing an EUV deficit that is correlated with  $Q(t)$  (Punsly 2015). The degree of magnetization of the inner disk determines scaling

relations for jet power and the EUV decrement. In particular, based on Figure 4 of Punsly (2015), the EUV deficit and jet power of 3C 270.1 indicates that  $\approx 50\%$  of the innermost accretion flow is displaced by the magnetic islands.

### REFERENCES

- Akujor, C., et al. 1994, *Astron. & Astrophys. Suppl.* **105** 247  
Aldcroft, T., Bechtold, J., Elvis, M. 1994 *Astrophys. J. Suppl.* **95** 1  
Anderson, S., Weymann, R., Foltz, C., Chaffee, F. 1970 *Astron. J.* **94** 278  
Bachev, R., Marziani, P., Sulentic, J. W., et al. 2004, *Astrophys. J.* **617** 171  
Becker, R., et al. 2001 *Astrophys. J. Supp.* **135** 227  
Blundell, K., Rawlings, S. 2000 *Astron. J.* **119** 1111  
Cardelli, J., Clayton, G., Mathis, J. 1989 *Astrophys. J.* **345** 245  
Davis, S., Laor, A. 2011, *Astrophys. J.* **728** 98 245  
deVries, W., Becker, R., White, R. 2006, *Astron. J.* **131** 666  
Garrington, S., Conway, R., Leahy, J., 1991 *Mon. Not. R. Astr. Soc.* **250** 173  
Gibson, R. et al 2009 *Atrophys. J.* **692** 758  
Gregg, M., Becker, R., de Vries, W., 2006 *Astrophys. J.* **641** 210  
Jackson, N., Rawlings, S. 1997 *Mon. Not. R. Astr. Soc.* **286** 241  
Knigge, C., Scaringi, S., Goad, M., Cottis, C. 2008 *Mon. Not. R. Astr. Soc.* **386** 1426  
Laor, A., Davis, S. 2014 *Astrophys. J.* **428** 3024  
Lonsdale, C., Barthel, P., Miley, G. 1993 *Astrophys. J. Supp.* **87** 63  
Punsly, B. 2005 *Astrophys. J. Lett.* **623** 9  
Punsly, B. 2006 *Astrophys. J.* **647** 886  
Punsly, B. 2007 *Mon. Not. R. Astr. Soc. Lett.* **374** 10  
Punsly, B. 2010 *Astrophys. J. Lett.* **713** 232  
Punsly, B. 2014 *Astrophys. J. Lett.* **797** 33  
Punsly, B. 2015 *Astrophys. J.* **806** 47  
Reid, A., et al. 1995 *Astron. & Astrophys. Suppl.* **110** 213  
Richards, G. et al. 2011 *Astron. J.* **141** 167  
Shankar, F., Dai, X., Sivakoff, G., 2008 *Astrophys. J.* **687** 859  
Shen, Y., & Liu, X. 2012, *Astrophys. J.* **753** 125  
Shull, M., Stevans, M., Danforth, C. 2012 *Astrophys. J.* **752** 162  
Sulentic, J. W., Bachev, R., Marziani, P., Negrete, C. A., & Dultzin, D. 2007, *Astrophys. J.*, **666**, 757  
Telfer, R., Zheng, W., Kriss, G., Davidsen, A. 2002 *Astrophys. J.* **565** 773  
Trakhtenbrot, B. and Netzer, H. 2012, *Mon. Not. R. Astr. Soc.* **427**, 3081

6 *Brian Punsly and Paola Marziani*

- Weymann, R.J., Morris, S.L., Foltz, C.B., Hewett, P.C.  
1991, *Astrophys. J.* **373**, 23
- Willott, C., Rawlings, S., Blundell, K., Lacy, M. 1999 *Mon.  
Not. R. Astr. Soc.* **309** 1017
- Wills, B. et al 1995, *Astrophys. J.* **437** 139
- Zheng, W. et al. 1997 *Astrophys. J.* **475** 469